Citation: Qiuping Zheng, Ting Chen, Yingli Wang, et al. Discharge behaviors of supercritical N_2 under direct-current electric field. *Journal of Harbin Institute of Technology (New Series)*. DOI: 10.11916/j.issn.1005-9113.24038

Discharge Behaviors of Supercritical N_2 under Direct-current Electric Field

Qiuping Zheng[1], Ting Chen[2*], Yingli Wang[3], Dongyue Cao[3], Haitao Hu[4] and Dianchun Zheng[2]*

(*1. Instrumentation Technology & Economy Institute, Beijing 100055, China;*
2. School of Electrical and Electronic Engineering, Harbin University of Science and Technology, Harbin 150080, China;
3. School of Measurement and Communication, Harbin University of Science and Technology, Harbin 150080, China;
4. Network Information Center, Harbin University of Science and Technology, Harbin 150080, China)

Abstract: The precise mathematical method was adopted to simulate the breakdown process of 5 mm rod and plate electrode gap, which was filled with supercritical nitrogen at the condition of 127 K, 4 MPa and seed electron density 1×10^6 m^{-3} under 29 kV DC voltage. The result shows that the discharge process was completed within 11.8 ns from seed electron triggering, avalanche bulking to streamer extending until gap eventually breakdown. The entire gap breakdown process was divided into three discharge stages, namely, the initial discharge triggered (0-4 ns), avalanche (4-7 ns) and streamer phase (7-11.8 ns). At the same time, the facts were also revealed that the discharge evolution, electric field distribution, and electron density had different values, and also showed different temporal and spatial distribution characteristics along the axis of the discharge gap. Specifically, the discharge characteristics of SCN_2 under 1, 2, 3, 4, 4.5, and 5 MPa at 127 K were theoretically analyzed respectively, and the microscopic mechanisms of the breakdown process were also detailed. The results indicate that the gas discharge law remained applicable within the 1-3 MPa range. However, the discharge characteristics of supercritical nitrogen at 3.4-5 MPa differed significantly from those at lower pressures, likely attributable to the unique state of matter exhibited by supercritical nitrogen. This study contributes to understanding the discharge mechanism of supercritical nitrogen and offers theoretical guidance for its practical application in the power industry.

Keywords: SCN_2; discharge behavior; avalanche; streamer; clusters
CLC number: TM855 **Document code**: A **Article ID**: 1005-9113(2025)00-0000-09

0 Introduction

Sulfur hexafluoride (SF_6), renowned for its superior dielectric performance, has become the predominant insulating dielectric in high-voltage electrical systems and power equipment application domain. However, owing to the greenhouse effect, SF_6 has been designated by the Kyoto Protocol as one of the six greenhouse gases. So far, scientists around the world have tried their best for decades to find a way to replace sulfur hexafluoride gas, but have not yet achieved the desired results. Because no matter the sulfur hexafluor-based binary and ternary mixed gas, or the perfluorocarbon-based binary and ternary mixed one, their electrical insulation properties and costs are far from comparable to those of sulfur hexafluoride gas[1]. More important, these gases still contain fluorine elements, which may be a severe potential threat to the human living environment, and moreover, it is unknown up to now whether the derivatives of these gases dissociated under natural conditions are harmful to the earth's ecosystem and to the degree of harm[2]. In recent years, these electrical characteristics of air have attracted the attention of scholars, prompting relevant scientific research to get inspiration from them and find an environmentally friendly gas dielectric. Furthermore, biggest advantage of the global warming potential (GWP) of nitrogen is zero, which accounts for 78.1% of the volume in the air. Therefore, nitrogen may become one of the alternatives to sulfur hexafluoride gas, and its

Received 2024-07-03.
Sponsored by the National Natural Science Foundation of China (Grant No.51077032).
* Corresponding author: Qiuping Zheng, M.E., Senior Engineer, Email: zhengqiupingnicole@hotmail.com; Ting Chen, D.E., Senior Engineer, Email: chenting@hrbust.edu.cn.

electrical characteristics are of great concern to scientists.

Supercritical nitrogen (SCN_2) has emerged as a focal point in scientific research due to its promising potential for advancing high-voltage electrical insulation systems. Recent investigations have progressively elucidated the dielectric behavior of SCN_2. Notably, Markosyan et al.[3] systematically characterized breakdown mechanisms in SCN_2 under 8 MPa/290 K conditions, establishing quantitative correlations between dielectric strength and thermodynamic parameters (pressure-temperature interdependence). Sun et al.[4] employed three-dimensional particle-in-cell (PIC) simulations to investigate SCN_2 dynamics in needle electrode configurations, elucidating the critical transition mechanisms from avalanche-to-streamer discharge through multi-physics coupling analysis. Zhang et al.[5-7] developed a comprehensive model for the SCN_2 insulated switch and systematically investigated its insulation breakdown and recovery characteristics under high-voltage conditions of 30 kV at a frequency of 1 kHz . Subsequently, Hou et al.[8] conducted a theoretical analysis of the molecular-dynamic behavior and molecular cluster distribution in SCN_2 under DC electric fields. Ashutosh et al.[9] performed numerical simulations of SCN_2 breakdown characteristics using a two-dimensional computational approach. The results demonstrated that the discharge process in short-gap SCN_2 configurations is a synergistic effect of the compound field strength and thermal energy. Dai et al.[10] conducted a theoretical investigation to discover the discharge mechanism of SCN_2 at the critical point (127 K, 3.4 MPa). Utilizing the BOLSIG+ software, authors numerically quantified major parameters governing the discharge behavior of SCN_2. Additionally, through molecular dynamics simulations, Liu et al.[11] systematically analyzed the dynamic clustering characteristics of SCN_2. These computational results revealed the distinctive phenomena within a wide range of reduced electric fields (50-500 Td), and demonstrating the evolution process of electron clusters related to the electric field.

Currently, our research group is conducting experimental investigations on the discharge mechanisms of supercritical fluids under non-uniform electric field conditions. This article is structured as follows: Section 1 provides a concise overview of the current research landscape regarding the electrical properties of SCN_2, Section 2 establishes the theoretical framework and computational methodology for analyzing SCN_2 discharge characteristics, Section 3 presents a detailed analysis of SCN_2 discharge dynamics in DC non-uniform electric fields, with emphasis on process evolution, and Section 4 concludes with the key findings and implications derived from this investigation.

1 Model Description of SCN_2 Discharge

To enable an in-depth investigation of SCN_2 discharge characteristics and elucidate its breakdown mechanisms, we developed a rod-plane electrode configuration with the specifications shown in Fig. 1. A copper rod with a 0.5 mm tip radius and polished surface is taken as an electrode ,the grounded circular plate is another electrode (50 mm diameter) featuring chamfered edges, with an interelectrode gap distance of 5 mm between the rod apex and plane surface and direct voltage of 29 kV applied to the rod electrode. The system is modeled within an axisymmetric rotating cylindrical containment vessel[12], maintaining SCN_2 at its critical thermodynamic state (4 MPa pressure, 127 K temperature). This configuration facilitates controlled analysis of discharge dynamics under non-uniform electric field conditions.

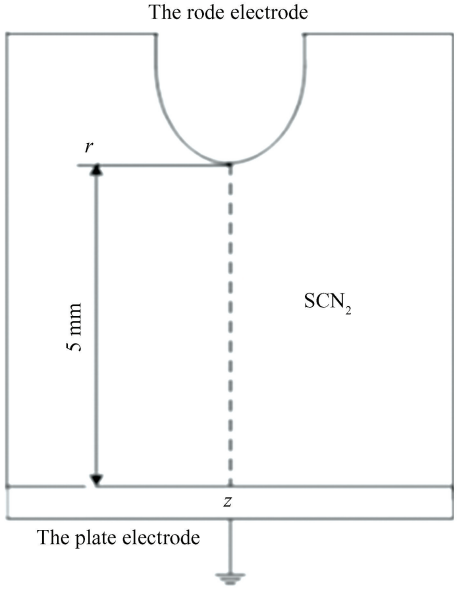

Fig. 1 Model diagram of rod-plate electrode

1.1 Governing Equations

In order to accurately depict the discharge physicochemical kinetics behavior of the model shown

in Fig.1, we use the first-order reaction-drift-diffusion model in local field approximation to account for the electron movement, generation and loss, and positive ion development in the discharge channel, which is coupled to Poisson's equation including the effect of space charge[13], the specific form is expressed as follows[14]:

$$\frac{\partial N_e}{\partial t} = S_e + \nabla \cdot (N_e \mu_e \boldsymbol{E} + D_e \nabla N_e) \tag{1}$$

$$\frac{\partial N_p}{\partial t} = S_e - \nabla \cdot (N_p \mu_p \boldsymbol{E} - D_p \nabla N_p) \tag{2}$$

$$\nabla^2 \phi = -\frac{e}{\varepsilon_0}(N_p - N_e) \tag{3}$$

$$\boldsymbol{E} = -\nabla \phi \tag{4}$$

where, N_e and N_p denote the number density of electron and positive ion, respectively. $\boldsymbol{E}$ represents the electric field intensity, ϕ represents the electric potential and e is the elementary charge quantity. The mobilities (and diffusion coefficients) of electrons and positive ions are denoted by μ_e (and D_e) and μ_p (and D_p), respectively, they are assumed to be functions of the reduced electric field E/N, N is the gas number density. S_e is a source term caused by photoionization in local field approximation, and is given as follows:

$$S_e(z) = \gamma_p \int_0^d \Omega(z - z') N_e(z') \alpha^*(z') |v(z')| \times \exp(-\mu |z - z'|) \mathrm{d}z' \tag{5}$$

where γ_p, α^*, and μ are second ionization, excitation and absorption coefficients for photoionization, and v is the velocity of the charged particle. Ω is the solid angle subtended at z' by the disk charge at z, a detailed solution about S_e has been introduced in Ref. [15]. The mobilities (and diffusion coefficients) of electrons and positive ions are denoted by μ_e (and D_e) and μ_p (and D_p), respectively, they are all assumed to be functions of the reduced electric field E/N, and their physical principles and calculation methods are described in detail in Ref. [16] and will not be discussed here.

At the cathode (plate electrode, i.e. line B, refer to Fig.2), electron values, depending on the secondary emission coefficient, are gained due to the ion impact on the earthed plate, as follows:

$$N_e|_B = \gamma N_p \tag{6}$$

where γ denotes the secondary emission coefficient and its value is taken as 0.07 in this work. In order to solve the simultaneous equations of SCN$_2$ (Eqs. (1) – (4)) smoothly, the compressible Euler equations without viscosity were adopted in the studies proposed by Tholin and Riousset[17-18].

1.2 Constraint Conditions

The computational framework employs a three-dimensional cylindrical coordinate system with axisymmetric approximation about the discharge axis (z-axis), effectively reducing the spatial dimensions through rotational symmetry, and supercritical N_2 at a temperature of 127 K and a pressure of 4 MPa is filled in vessel and maintained steadily. The calculation domain is shown in Fig. 2.

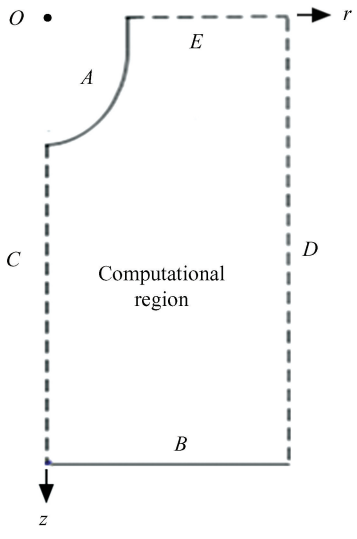

Fig.2 Diagram of computational domain

1) Boundary constraint of constant electric field.

A direct voltage is applied to the arc line A of the rod electrode while the plate electrode line B earthed, so their constraints are respectively expressed as follows:

$$\phi_A = U,\ \phi_B = 0$$

Based on the principle of constant electric field and axisymmetric field characteristics, so both line C and line D belong to the homogeneous Neumann boundary condition, the details are as follows:

$$\left.\frac{\partial \phi}{\partial z}\right|_C \approx 0, \left.\frac{\partial \phi}{\partial z}\right|_D \approx 0$$

Regarding line B, we only considered the effect of the secondary emission, so the Dirichlet boundary was imposed on the cathode plate, the detailed method refers to Eq. (6).

2) Constraints on charged particles.

The boundary constraint condition for the C-line along the field symmetry axis is defined as follows:

$$\left.\frac{\partial N_e}{\partial z}\right|_C = 0, \left.\frac{\partial N_p}{\partial z}\right|_C = 0$$

Therefore, the D-line and E-line constitute adiabatic boundaries corresponding to convective flux conditions, governed by the following equations:

$$\begin{cases} \boldsymbol{n} \cdot (-D_e \nabla N_e)|_D = 0 \\ \boldsymbol{n} \cdot (-D_p \nabla N_p)|_D = 0 \end{cases}$$

$$\begin{cases} \boldsymbol{n} \cdot (-D_e \nabla N_e)|_E = 0 \\ \boldsymbol{n} \cdot (-D_p \nabla N_p)|_E = 0 \end{cases}$$

Select the electron distribution in the form of Gaussian distribution as the initial seed electron source, and the function form is expressed as follows[19]:

$$N_e(r,z)|_{t=0} = N_0 \exp\{-((r-r_0)/\delta_r)^2 - ((z-z_0)/\delta_z)^2\}$$

where, r_0 and z_0 are the initial positions of the electron clusters located in the coordinate system. In this study, the center of the initial electron cluster is located 2 mm along the z-axis direction. δ_r and δ_z are the cluster radii of the initial seed electron respectively, and both values are equal to 0.25 μm. N_0 is the initial electron number density and the value is equal to 1×10^6 m^{-3}.

1.3 FCT Algorithm

The gas discharge process is generally recognized to progress through three distinct evolutionary phases: initial electron avalanches develop into space charge-dominated streamers, which subsequently transition to thermally-dominated leaders or arc discharges. Extensive experimental investigations and theoretical modeling efforts have been conducted to characterize this complex physical progression. A critical mechanism driving streamer propagation lies in space charge effects, where localized electric field enhancement at the streamer front facilitates sustained ionization processes. This self-reinforcing mechanism ultimately leads to dielectric breakdown of the medium through cumulative ionization activity[20]. Numerical analysis of such strongly nonlinear phenomena presents significant computational challenges, particularly in resolving the steep gradients at propagating streamer heads. The flux-corrected transport (FCT) technique has emerged as an effective computational framework for solving the coupled transport equations under these space-charge dominated conditions. Demonstrated through multiple validation studies[21-22], this algorithm maintains numerical stability while accurately resolving abrupt density variations characteristic of discharge dynamics. Eqs. (1) and (2) can be numerically integrated using finite difference technique. The accuracy of the method depends upon the order of the difference scheme. Higher order (second and above) schemes produce ripples near steep gradients. Lower order schemes such as donor cell do not produce ripples but suffer from excessive numerical diffusion. The flux corrected transport constructs the net transportive flux point by point as a weighted average of a flux computed by a low order scheme and a flux computed by a high order scheme. The weighting is done so that the high order flux is used to the greatest extent possible without introducing false ripples. Further details and calculation procedure on the FCT can be found in Ref.[23].

2 Results and Discussion

Through the above-mentioned rigorous simulations, the fascinating discharge characteristics of SCN_2 at 4 MPa and 127 K have been obtained. This result is conducive to a better understanding and revelation of its electrical discharge mechanism.

2.1 Distribution of Electrons

The time-space characteristics of the electron density of SCN_2 during the discharge process are illustrated in Fig. 3. These characteristics can be categorized into the following three phases:

1) Triggering initial discharge. Place the initial seed electron cluster (with a Gaussian distribution and a density of 1×10^6 m^{-3}) along the axis 2 mm away from the tip of the rod electrode. The external applied electric field is denoted by E_{ap} and the electric field created by the electron cluster is presented by E_e. The seed electrons move quickly away from the direction of the external electric field E_{ap} and toward the rod electrode while an external electric field is established. In such a short time, owing to the effect of an external electric field, the electron collides with a neutral nitrogen molecule, forming an electron and ion mixed cluster. Under the external electric field force, the cluster is quickly stretched along the E_{ap} directions, and at the same time, the initial discharge of the gap is triggered, so-called initial avalanche appeared. It is evident from Fig.3 that the electron density markedly increases within 3 ns period, and quickly up to 4.0092×10^{19} m^{-3}.

2) Discharge of avalanche phase. As shown in Fig.3, the peak value of electron densities increases up to 2.1902×10^{20} m^{-3} at the 4 ns moment. From this

point until the 7 ns period, the electron density at the head of the avalanche remained almost constant at around 10 to the power of 20. During this period, not only the electron density increases slightly, but also the avalanche bulk increases rapidly and the development speed of the discharge channel is also accelerated.

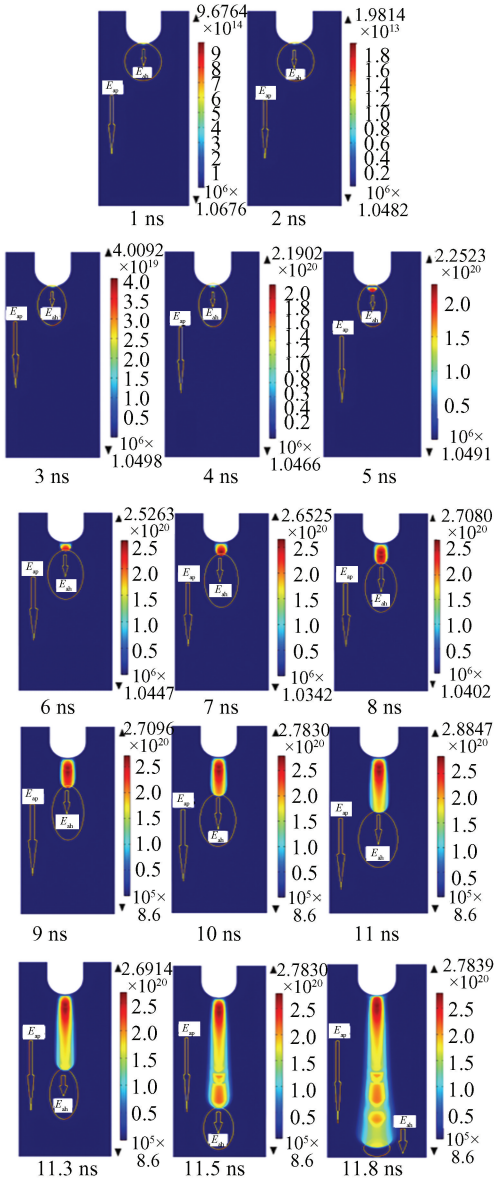

Fig. 3 Evolution process of SCN_2 discharge channel in the rod-plate gap

3) Discharge of streamer phase. As can be seen from Fig.3, 7 ns is the dividing line between avalanche and streamer discharge stage. From this moment on, electron density exponentially doubles, streamer volume rapidly also expands, and the speed of discharge development quickly accelerates until the electron density of the streamer head reaches 2.7839×10^{20} m^{-3} at 11.8 ns, the streamer bridges the gap of rod-plate electrode. The temporal distributions of electron concentration in the SCN_2 gap, which is from the apex of the rod end to the plate electrode along the axis of symmetry, are shown in Fig.4.

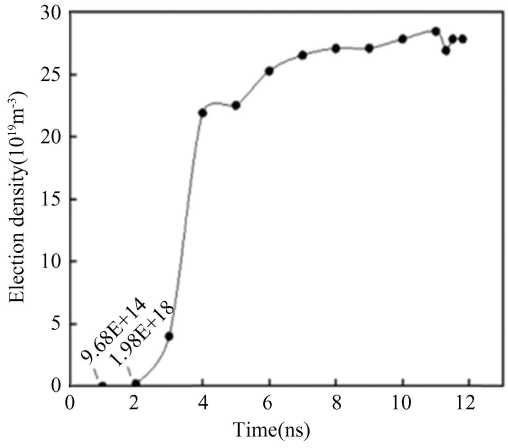

Fig.4 Curve between electron densities and time of SCN_2 gap discharge with rod-plate electrode

2.2 Evolution of Discharge Channel

Electric field distributions of the rod-plate gap at different moments along the discharge channel axis are shown in Fig.5. The peak values of the electric field strength reaches 1.0×10^7 V/m order of magnitude during the period of 0-3 ns, and the fact could be seen that the field strength slightly increases only near the rod-tip within small narrow region. Meanwhile, the electric field intensity E_{ah} at 4 ns is 1.2×10^7 V/m, and the electron density of the avalanche head is up to 2.1902×10^{20} m^{-3}, as mentioned earlier, and as marked by ① in Fig.5. Furthermore, when avalanche suddenly switches into the streamer phase, the event happens at 7 ns moment, at this very time, the electric field intensity E_{ah} is 1.8×10^7 V/m and electron density reaches 2.6525×10^{20} m^{-3} of order of magnitudes, happening position located about at 0.0005 m away from electrode rod vertex, as marked by ② in Fig. 5. What also happened next just as Marked by ③ in Fig. 5. The strongest electric field value E_{ah} almost reaches 1.9×10^7 V/m and appeares at a location 0.0045 m away from the plate electrode, indicating that a streamer head had nearly arrived at the plate electrode, and the peak value of electron density in the streamer head nearly goes up to 2.7839×10^{20} m^{-3}. Namely, the discharge plasma channel formed by avalanche and streamer has completely bridged the gap of the rod-plate.

An important fact demonstrated in Fig.4 is that the collision ionization of SCN_2 molecules with electrons activity occurs in the first 3 ns. That is because the electric field is not very strong, so these electrons do not have enough kinetic energy to actually collide with the molecules, then the growth rate of the avalanche bulk is also not quick along the discharge channel during this period.

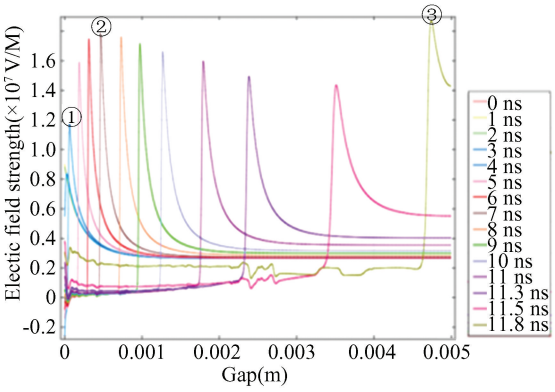

Fig.5 Distribution ofelectric field along the axis at different moment

And subsequently, the period from 4 to 7 ns is the development stage of avalanche discharge. However, the avalanche discharge is converted into a streamer phase at 7 ns, the speed of streamer development and propagation increase rapidly, as shown in Fig.3, the SCN_2 gap is breakdown eventually at 11.8 ns.

2.3 Generating Process of Charged Particles

Based on the results shown in Fig. 3 and Fig. 5, these facts are proven that the discharge process of SCN_2 with a gap of 5 mm involves three stages: a) discharge triggering, b) avalanche discharge stage and c) streamer discharge stage. At the same time, the following three reactions occur under the excitation of an external electric field[24-25].

1) Electron collision ionization reaction with N_2 molecule(as shown in Table 1).

Table 1 Electron collision ionization reaction with N_2 molecule

No.	Reaction mode	Rate const($cm^3 \cdot s^{-1}$)	Electric field intensity E_{ah}(V/m)
1	$e+N_2 \rightarrow e+N+N$	2.0×10^{-11}	$1.155\times10^7<E_{ah}<1.8\times10^7$
2	$e+N_2 \rightarrow 2e+N^++N$	2.4×10^{-17}	$1.175\times10^7<E_{ah}<1.8\times10^9$
3	$e+N_2 \rightarrow 2e+N_2^+$	2.4×10^{-12}	$1.185\times10^7<E_{ah}<1.8\times10^{10}$

2) Electron-ion recombining reaction(as shown in Table 2).

Table 2 Electron-ion recombining reaction

No.	Reaction mode	Rate const($cm^3 \cdot s^{-1}$)	Electric field intensity E_{ah}(V/m)
1	$N^++e+M\rightarrow N+M$	$3.5\times10^{-12}(300/T)^{0.7}+6.0\times10^{-27}(300/T)^{25}M$	$1.155\times10^7<E_{ah}<1.8\times10^7$
2	$N_2^++e\rightarrow N+N$	$2.8\times10^{-7}(300/T)^{0.5}$	$1.175\times10^7<E_{ah}<1.8\times10^9$
3	$N_2^++e+M\rightarrow N_2+M$	$4.0\times10^{-12}(300/T)^{0.7}+6.0\times10^{-27}(300/T)^{25}M$	$1.185\times10^7<E_{ah}<1.8\times10^{10}$

3) Electron exchange and ion conversion reactions(as shown in Table 3).

Table 3 Electron exchange and ion conversion reactions

No.	Reaction mode	Rate const($cm^3 \cdot s^{-1}$)	Electric field intensity E_{ah}(V/m)
1	$N_2^++N\rightarrow N_2+N^+$	1.0×10^{-11}	$1.185\times10^7<E_{ah}<1.8\times10^{10}$

Furthermore, the excitation, ionization and recombination of SCN_2 molecules under electric field force run through the entire process of rod-plate gap discharge. Because as long as electrons obtain sufficient energy from the electric field, the ionization occurs from the ground state $N_2(X^1\sum_g^+,\nu)$ molecule as follows:

$$e^- + N_2(X^1\sum_g^+,\nu) + N_2^+(X^2\sum_g^+,\nu') + 2e^-$$

$$e^- + N_2(X^1\sum_g^+,\nu) + N_2^+(B^2\sum_u^+,\nu') + 2e^-$$

$$e^- + N_2(X^1\sum_g^+,\nu) + N_2^+(C^2\sum_g^+,\nu') + 2e^-$$

Naturally, there are also direct excitations by electron impact from the ground state which require less energy than that of the ionization [26]:

$$e^- + N_2(X^1\sum_g^+,\nu) + N_2^+(A^3\sum_u^+,\nu') + e^-$$

$$e^- + N_2(X^1\sum_g^+,\nu) + N_2^+(B^3\pi_g,\nu') + e^-$$

$$e^- + N_2(X^1\sum_g^+,\nu) + N_2^+(C^3\pi_u,\nu') + e^-$$

In summary, in the process of gap discharge, due to the intensification of gap electric field distortion, the energy transfer between charged particles and the effect of photoionization, the triggering discharge develops from electron collapse formation, and then transforms into stream discharge until the gap breakdown eventually. Therefore, electron-molecular impact ionization, electron-ion recombination, electron exchange and ion conversion reactions take place through any point in the

spatiotemporal scale of the SCN_2 discharge trajectory within the rod-plate electrode.

3 Breakdown Characteristic of SCN_2

In order to reveal the breakdown characteristics of the SCN_2 under DC nonuniform electric field, following the method described herein, keeping the electrode configuration intact and maintaining the temperatures at 127 K constant, the breakdown field strength of SCN_2 was numerically calculated (as shown in Fig.6) while the pressures ranged from 1 to 5 MPa. Meanwhile, their microscopic parameters of gap discharge are listed in Table 4.

In Table 4, V_{br} is the value of breakdown voltage applied to rod-plate electrode system; T_{br} is the time of thoroughly breakdown of SCN_2 gap; T_{ah} denotes the period of avalanche phase and the moment of transiting avalanche into streamer; D_{ah} stands for electron density of the avalanche while being changed into streamer; L_{ah} represents the distance of the avalanche head apart from the rod electrode when the avalanche being changed into streamer; $E_{max}(L)_{loc}$ denotes the maximum field intensity within the discharge gap; D_{sl} stands for the electron density of the streamer nearest plate electrode.

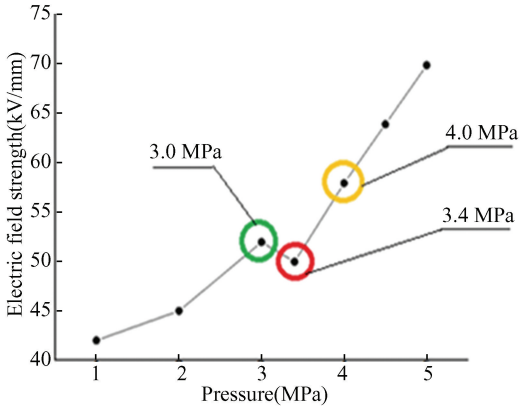

Fig.6 Relationship between breakdown field and pressure (1 to 5 MPa) at 127 K

Table 4 SCN_2 gap discharge parameters under 1 to 5 MPa at 127 K

P (MPa)	V_{br} (kV)	T_{br} (ns)	T_{ah} (ns)	D_{ah} (m^3)	L_{ah} (m)	$E_{max}(L)_{loc}$	D_{sl} (m^2)
1.0	12.5	9.0	5.0/9.0	2.2791×10^{19}	0.00008	4.250×10^6(0.00450)	1.68770×10^{19}
2.0	15.0	9.5	5.0/9.5	4.9572×10^{19}	0.00010	9.743×10^6(0.00470)	3.09280×10^{19}
3.0	26.0	10.6	3.0/5.0	2.0286×10^{18}	0.00030	1.430×10^7(0.00400)	2.00932×10^{20}
3.4	25.0	10.2	4.0/6.0	9.6300×10^{19}	0.00050	1.210×10^7(0.00070)	2.07180×10^{20}
4.0	29.0	11.8	3.0/6.0	4.0100×10^{19}	0.00010	1.850×10^7(0.00480)	2.78390×10^{20}
4.5	32.0	12.5	3.0/7.0	9.4835×10^{19}	0.00005	3.250×10^7(0.00485)	3.10730×10^{20}
5.0	35.0	13.4	2.0/6.0	2.1405×10^{18}	0.00010	3.850×10^7(0.00130)	3.34970×10^{20}

Fig.6 demonstrates the following facts: 1) When the temperature is 127 K and the pressure is 1, 2 and 3 MPa, the breakdown characteristics of gaseous nitrogen follow the classical theory. 2) When the temperature is 127 K and the pressure is 3.4, 4.0, 4.5 and 5.0 MPa, the breakdown characteristics of nitrogen under supercritical conditions seem to be consistent with the classical discharge law, but its mechanism needs further theoretical investigation and experimental verification. 3) However, at the supercritical point (127 K and 3.4 MPa), there is a slight decrease in the breakdown field strength, this may be a specific physical property of SCN_2. In other words, the supercritical point of nitrogen is the inflection point of breakdown electric field, and it might depend on the molecular structure of the supercritical substance. This special phenomenon is possible due to the local ionizing enhancement caused by N_2 cluster degree, resulting in the free path of the electron being shortened, and the energy accumulation of the electron being hindered. In the supercritical state of N_2, the formation of molecular clusters usually gives rise to local inhomogeneity in the density of SCN_2, accompanied by a significant enhancement of the local density. Consequently, electrons are unable to acquire sufficient energy to induce collision ionization. Moreover, the molecular clusters may also reduce the molecular ionization energy, as reported in Refs. [27-28].

4 Conclusions

The precise mathematical algorithm was applied to modeling the breakdown process of the 5 mm rod-plate SCN_2 gap under the condition of 127 K, 4.0 MPa, seed electron density of 1×10^6 m^{-3}, and an

applied DC voltage of 29 kV in this study. The achievements obtained are as follows:

1) During 0-3 ns, it was the avalanche triggering discharge process and 4-7 ns period is the growth of avalanche bulk;

2) At 7 ns, it was a critical point that the avalanche phase was instant into streamer phase, causing the gap to breakdown instantaneously;

3) The electron density distribution and discharge trajectory evolution parameters of the discharge gap were obtained, as shown in Fig.3.

4) The characteristics and parameters of non-uniform electric field discharge in 5 mm gap of SCN_2 at constant value of 127 K and pressure ranging from 1 to 5 MPa were obtained through rigorous theoretical analysis, as shown in Table 1.

5) In particular, the discharge characteristics of SCN_2 at 127 K, pressures of 3.4, 4.0, 4.5 and 5.0 MPa and 5 mm non-uniform electric fields, the kinetic behavior of charged particles, the process of molecular ionization and the evolution history of discharge trajectory were obtained theoretically for the first time. The research results obtained in this study would contribute to further scientific investigation in this field, and provide effective research methods and theoretical basis for further development of green environmental protection dielectrics.

Acknowledgements:

The authors sincerely thank the experts from the Computing Center of the School of Electrical Engineering for their support of this project.

References

[1] Kieffel Y, Irwin T, Ponchon P, et al. Green gas to replace SF_6 in electrical grids. IEEE, Power & Energy Magazine, 2016, 14(2): 32-39. DOI: 10.1109/MPE.2016.2542645.

[2] Chu F Y. SF_6 decomposition in gas-insulated quipment. IEEE Transactions on Electrical Insulation, 1986, EI-21(5): 693-725. DOI: 10.1109/TEI.1986.348921.

[3] Markosyan A H, Zhang J, van Heesch E J M, et al. Streamer to spark transition in supercritical N_2. 20th Symposium on Physics of Switching Arc (FSO 2013). Brno: FSO, 2013: 2-6.

[4] Sun A, Teunissen J, Ebert U. 3-D particle modeling of positive streamer inception from a needle electrode in supercritical nitrogen. IEEE Transactions on Plasma Science, 2014, 42(10): 2416-2417. DOI: 10.1109/TPS.2014.2308724.

[5] Zhang J, Furusato T, Beckers F J C M, et al. Study of breakdown inside a supercritical fluid plasma switch. 2013 19th IEEE Pulsed Power Conference (PPC). Piscataway: IEEE, 2013: 1-5. DOI: 10.1109/PPC.2013.6627456.

[6] Zhang J, van Heesch B, Beckers F, et al. Breakdown voltage and recovery rate estimation of a supercritical nitrogen plasma switch. IEEE Transactions on Plasma Science, 2014, 42(2): 376-383. DOI: 10.1109/TPS.2013.2294756.

[7] Zhang J, Markosyan A H, Seeger M, et al. Numerical and experimental investigation of dielectric recovery in supercritical N_2. Plasma Sources Science and Technology, 2015, 24(2): 1-27. DOI: 10.1088/0963-0252/24/2/025008

[8] Hou P J, Zheng D C, Zhao D, et al. Application of supercritical nitrogen as a promising medium in electric equipment. 2015 3rd International Conference on Electric Power Equipment-Switching Technology (ICEPE-ST). Busan, 2015: 325-328. DOI: 10.1109/ICEPE-ST.2015.7368396.

[9] Agnihotri A, Hundsdorfer W, Ebert U. Coupling discharge and gas dynamics in streamer-less spark formation in supercritical N_2. Japanese Journal of Applied Physics, 2016, 55: 07LD06-1-07LD06-4. DOI: 10.7567/JJAP.55.07LD06

[10] Dai X L, Chen C T, Wei H Q, et al. Electron impact ionization, attachment, drift velocities and longitudinal diffusion of SCN_2 at the critical point 127 K and 3.4 MPa. 2019 5th International Conference on Electric Power Equipment-Switching Technology (ICEPE-ST). Kitakyushu, 2019: 762-766. DOI: 10.1109/ICEPE-ST.2019.8928773.

[11] Liu Z Y, Wei H Q, Zhao D W, et al. Research on the discharge behaviors of SCN_2. 2017 4th International Conference on Electric Power Equipment-Switching Technology (ICEPE-ST). Xi'an, 2017: 44. DOI: 10.1109/ICEPE-ST.2017.8188847.

[12] Zheng Q P, Chen T, Hu H T, et al. Research on intelligent identification of PD patterns based on the fingerprint features. Applied Mathematics, 2022, 13: 896-916.

[13] Zheng D C, Wang J, Chen C T, et al. Dynamic characteristics of SF6-N_2-CO_2 gas mixtures in DC discharge process. Plasma Science and Technology, 2014, 16(9): 848-855. DOI: 10.1088/1009-0630/16/9/08.

[14] Agnihotri A. Modeling heat dominated electrical breakdown. Eindhoven: Eindhoven University of Technology, 2018.

[15] Morrow R. Theory of positive corona in SF_6 due to a voltage impulse. IEEE Trans on Plasma Science, 1991, 19(2): 86-94. DOI: 10.1109/27.106801.

[16] Hagelaar G J M, Pitchford L C. Solving the Boltzmann equation to obtain electron transport coefficients and rate coefficients for fluid models. Plasma Sources Science and Technology, 2005, 14: 722-733. DOI: 10.1088/0963-0252/14/4/011.

[17] Tholin F, Bourdon A. Simulation of the hydrodynamic

expansion following a nanosecond pulsed spark discharge in air at atmospheric pressure. Journal of Physics D: Applied Physics, 2013, 46(36): 365205. DOI: 10.1088/0022-3727/46/36/365205.

[18] Riousset J A, Pasko V P, Bourdon A. Air-density-dependent model for analysis of air heating associated with streamers, leaders, and transient luminous events. Journal of Geophysical Research: Space Physics, 2010, 115(12): A12321.

[19] Zheng D C. Dielectric Properties and Applications of SF_6. Beijing: Science Press, 2019.

[20] Popov N A. Formation and development of a leader channel in air. Plasma Physics Reports, 2003, 29(8): 695-708. DOI: 10.1134/1.1601648.

[21] Montijn C, Ebert U. Diffusion correction to the Raether-Meek criterion for the avalanche-to-streamer transition. Journal of Physics D: Applied Physics, 2006, 39: 2979. DOI: 10.1088/0022-3727/39/14/017.

[22] Zheng Dianchun, Xia Yunsuang, Zhu Shihua et al. Dynamics simulation of SF_6 discharge in a short gap under uniform electric field. Chinese Journal of Computational Physics, 2012, 29(6): 865-875.

[23] Zheng Q P, Zheng D C. Mathematical modeling on dynamic characteristics of the breakdown process in narrow-gap of SF_6 based on the FCT algorithm. Applied Mathematics, 2019, 10(9): 769-783. DOI: 10.4236/am.2019.109055.

[24] Nijdam S, Takahashi E, Markosyan A H, et al. Investigation of positive streamers by double-pulse experiments, effects of repetition rate and gas mixture. Plasma Sources Science and Technology, 2014, 23(2): 025008. DOI: 10.1088/0963-0252/23/2/025008.

[25] Hagelaar G J M, Pitchford L C. Solving the Boltzmann equation to obtain electron transport coefficients and rate coefficients for fluid models. Plasma Sources Science and Technology, 2005, 14(4): 722. DOI: 10.1088/0963-0252/14/4/011.

[26] Potamianou S, Spyrou N, Held B, et al. Numerical study of active particles creation and evolution in a nitrogen point-to-plane afterglow discharge at low pressure. Journal of Physics D: Applied Physics, 2006, 39(18): 4001-4009. DOI: 10.1088/0022-3727/39/18/012.

[27] Abahazem A, Merbahi N, Guedah H, et al. Electric and spectroscopic studies of pulsed corona discharges in nitrogen at atmospheric pressure. Journal of Analytical Sciences, Methods and Instrumentation, 2017, 7: 57-74. DOI: 10.4236/jasmi.2017.73006.

[28] Wei H Q. Study on Discharge Characteristics of Supercritical Nitrogen. Harbin: Harbin University of Science and Technology, 2017.